Surface ozone at Nam Co in the inland Tibetan Plateau: variation, synthesis comparison and regional representativeness

Xiufeng Yin [1, 2, 3], Shichang Kang [1, 4], Benjamin de Foy [5], Zhiyuan Cong [2, 4], Jiali Luo [6], Lang Zhang [2], Yaoming Ma [2, 4], Guoshuai Zhang [2], Dipesh Rupakheti [2, 3], Qianggong Zhang [2, 4]

[1]State Key Laboratory of Cryospheric Sciences, Northwest Institute of Eco-Environment and Resources, Chinese Academy of Science, Lanzhou, 730000, China

[2] Key Laboratory of Tibetan Environment Changes and Land Surface Processes, Institute of Tibetan Plateau Research, Chinese Academy of Sciences, Beijing, 100101, China

[3]University of Chinese Academy of Sciences, Beijing, 100039, China

[4]CAS Center for Excellence in Tibetan Plateau Earth Sciences, Beijing, 100085, China

[5]Department of Earth and Atmospheric Sciences, Saint Louis University, St. Louis, MO, 63108, USA

[6]Key Laboratory of Semi-Arid Climate Change, Ministry of Education, Lanzhou, 730000, China

Correspondence to: Qianggong Zhang (qianggong.zhang@itpcas.ac.cn) and Shichang Kang (shichang.kang@lzb.ac.cn)

Abstract:

Ozone is an important pollutant and greenhouse gas, and tropospheric ozone variations are generally associated with both natural and anthropogenic processes. As one of the most pristine and inaccessible regions in the world, the Tibetan Plateau has been considered as an ideal region for studying processes of the background atmosphere. Due to the vast area of the Tibetan Plateau, sites in the southern, northern and central regions exhibit different patterns of variation in surface ozone. Here, we present long-term measurements for ~5 years (January 2011 to October 2015) of surface ozone mixing ratios at Nam Co Station, which is a background site in the inland Tibetan Plateau. An average surface ozone mixing ratio of 47.6±11.6 ppb was recorded, and a large annual cycle was observed with maximum ozone mixing ratios in the spring and minimum ratios during the winter. The diurnal cycle is characterized by a minimum in the early morning and a maximum in the late afternoon. Nam Co Station represents a background region where surface ozone receives negligible local anthropogenic emissions. Surface ozone at Nam Co Station is mainly dominated by natural processes involving photochemical reactions, vertical mixing and stratospheric air mass downward transport. Model results indicate that the study site is affected by the surrounding areas in different seasons: air masses from the southern Tibetan Plateau contribute to the high ozone levels in the spring and enhanced ozone levels in the summer were associated with air masses from the northern Tibetan Plateau. By comparing measurements at Nam Co Station with those from other sites in the Tibetan Plateau, we aim to expand the understanding of ozone cycles and transport processes over the Tibetan Plateau. This work may provide a reference for model simulations in the future.

1 Introduction

The concentration of ozone in the troposphere showed sustained growth during the 20th century due to the increased emissions of anthropogenic precursors (Cooper et al., 2014). High levels of surface ozone are currently a major environmental concern because of the harm ozone poses to health and vegetation at the surface (LRTAP, 2015; REVIHAAP, 2013; US EPA, 2013; Mauzerall and Wang, 2001; Desqueyroux et al., 2002). In addition, ozone is a major precursor of hydroxyl (OH) and hydroperoxy (HO_2) radicals and it controls the oxidation capacity of the atmosphere (Brasseur et al., 1999). Furthermore, as the third most important greenhouse gas (after carbon dioxide (CO_2) and methane (CH_4)), tropospheric ozone contributes to global warming and has an estimated globally average radiative forcing of 0.40 ± 0.20 W m^{-2} with high confidence level (Myhre et al., 2013). For global modeling, monthly and annual average concentrations of tropospheric ozone are used for assessing and improving the modeling results (Wild and Prather, 2006; Roelofs et al., 2003).

The origin of tropospheric ozone and its temporal variation varies from site to site. Historically, the stratosphere was initially thought to be the main source of surface (tropospheric) ozone and a network of surface ozone monitoring sites was proposed (Junge, 1962). In the 1970s and 1980s, the effect of photochemical reactions in the troposphere on surface ozone became well recognized (Chameides and Walker, 1973; Crutzen, 1974) and photochemistry was identified as the dominant source of tropospheric ozone at some sites, as supported by models (Wu et al., 2007). Background sites can represent areas with surface ozone concentrations that are under the control of largely uniform synoptic systems and are minimally affected by local anthropogenic sources. The study of surface ozone at background sites may enrich the understanding of surface ozone variation patterns.

Due to its small human population and low level of industrialization, the Tibetan Plateau is an ideal natural laboratory for studying surface ozone across remote regions of the Eurasian continent. Long term surface ozone measurements over the Tibetan Plateau have been conducted at Mt. Waliguan (northeast edge of the Tibetan Plateau) since 1994 (Xu et al., 2016), the Nepal Climate Observatory at Pyramid (NCO-P) which operates on the southern slope of the Himalayan region since 2006 (Cristofanelli et al., 2010) and the Xianggelila Regional Atmosphere Background Station at the southeastern rim of the Tibetan Plateau since 2007 (Ma et al., 2014). Analysis of long-term ozone mixing ratios at Waliguan Station has revealed steadily increasing concentrations over the past two decades (Xu et al., 2016) and has shown that maximum surface ozone occurs during the summer (Zhu et al., 2004). At NCO-P and Xianggelila, surface ozone maximum was observed in the spring (Cristofanelli et al., 2010; Ma et al., 2014). It is noteworthy that these three monitoring sites are on the boundaries of the Tibetan Plateau. In the vast inland area of the Tibetan Plateau, surface ozone measurements were only reported from Lhasa

and Dangxiong for one year and two years, respectively. These measurements might be less representative of regional surface ozone variation due to their proximity to human settlements and relatively short duration of the measurements (Ran et al., 2014; Lin et al. 2015). The paucity of long-term surface ozone observations in the Tibetan Plateau, especially in the inland region, limits our understanding of the regional background ozone level and the factors that influence it and can potentially lead to inaccurate simulation of surface ozone variation over the Tibetan Plateau.

Surface ozone mixing ratios were monitored for ~5 years (January 2011 to October 2015) at Nam Co Station on the shore of Nam Co Lake (30°30′-30°56′N, 90°16′-91°03′E). In this study, we investigated the seasonal and diurnal variations of surface ozone and its influencing factors. We then evaluated surface ozone variability using combined observations over the Tibetan Plateau and beyond. Finally, we discussed the potential representativeness of surface ozone at Nam Co Station as the regional background of surface ozone in the inland Tibetan Plateau. This study expands the understanding of baseline and variations in the surface ozone concentration and the transport processes that influence tropospheric ozone in the inland Tibetan Plateau. The long-term measurements of surface ozone; together with other reported surface ozone time series over the Tibetan Plateau represent valuable datasets for evaluating long-term regional-scale ozone trends.

2 Measurements and Methods

2.1 Measurement site

The Tibetan Plateau (27°N–45°N, 70°E–105°E, average elevation ~ 4 km) is the highest and most extensive highland in the world and has been called the 'Third Pole' (Yao et al., 2012). The Nam Co Comprehensive Observation and Research Station (hereafter referred to as the Nam Co Station, 30°46.44′N, 90°59.31′E, 4730 m a.s.l.) is a high altitude scientific research center located between the southeast shore of Nam Co Lake (1 km from the station) and the foothills of the northern Nyainqêntanglha Mountains (15 km from the station) in the southern-central region of the Tibetan Plateau (Fig. 1). Nam Co Station was established to monitor atmospheric conditions in September 2005 and provided a long-term record of the atmospheric environment in the Tibetan Plateau (Kang et al., 2011). Nam Co Station is in a natural flat field (220 × 100 m) and records meteorological, ecological, and atmospheric data, including surface ozone mixing ratios (Cong et al., 2007; Li et al., 2007; Huang et al., 2012; Liu et al., 2015; de Foy et al., 2016a). The climate at Nam Co Station is dry and cold, representing a typical climate regime in the high mountain region. The solar radiation at Nam Co Station is stronger than that at other sites at the same latitude due to the high altitude and thin air. Three synoptic systems influence the atmosphere at Nam Co Station: the South Asian anticyclone (which controls the 100-hPa upper layer), a subtropical high-pressure system, and southeast warm and wet airflow (during the monsoon season) (Qiao and Zhang, 1994). No major anthropogenic sources of atmospheric

emissions exist near Nam Co Station. The urban area closest to the station is Dangxiong County, which is located on the southern slopes of the Nyainqêntanglha Mountain Range approximately 60 km south of Nam Co. Dangxiong is lower in elevation than Nam Co Station by more than 500 m. No large industries are located within 100 km of Nam Co Station. Local traffic is limited to a small number of vehicles traveling through the area during the tourist season.

2.2 Measurements: surface ozone and meteorology

The surface ozone mixing ratios were measured using a UV photometric instrument (Thermo Environmental Instruments, USA, Model 49i), which uses absorption of radiation at 254 nm and has a dual cell design. The ambient air inlet (Teflon tube) was 1.5 m above the roof and 4 m above the ground. The instrument has zero noise, 0.25 parts per billion (ppb) RMS (root mean square error) (60 s average time), a low detection limit of 0.5 ppb, a precision of 1 ppb and a response time of 20 s (10 s lag time). The instrument was calibrated using a 49i-PS calibrator (Thermo Environmental Instruments, USA) before measurements and during the monitoring periods and yearly instrument calibrations are performed against the Standard Reference Photometer (SRP) maintained by the WMO World Calibration Centre in Switzerland (EMPA). Field operators checked the instruments and created a monitoring log file every day. Due to the extreme winter weather that occurs at Nam Co Station, measurements were intermittently interrupted because of unstable power supply (due to damage from strong winds to the electrical wires) and equipment maintenance. All data displayed in this study are in UTC+8 (Beijing Time, BJT), and solar noon at Nam Co Station is at 13:56 in UTC+8.

Measurements of temperature, relative humidity, wind speed, wind direction and downward shortwave radiation (SWD) were conducted at Nam Co Station using an automatic weather station system (Milos520, Vaisala) and a radiation measurement system (CNR-1) (Ma et al., 2008).

2.3 Meteorological simulations

Backward trajectories and clusters were calculated by NOAA-HYSPLIT (HYbrid Single-Particle Lagrangian Integrated Trajectory) model (Draxler and Rolph, 2003, http://ready.arl.noaa.gov/HYSPLIT.php) using TrajStat, which is a free software plugin of MeteoInfo (Wang, 2014). Gridded meteorological data for backward trajectories in HYSPLIT and Planetary boundary layer height (PBLH) were obtained from Global Data Assimilation System (GDAS-1) by the U.S. National Oceanic and Atmospheric Administration (NOAA) with 1°×1° latitude and longitude horizontal resolution and vertical levels of 23 from 1000 hPa to 20 hPa (http: // www. arl. noaa. gov/ gdas1. php). The backward trajectories arrival height in HYSPLIT was set at 500 m (500 m, 1000 m and 1500 m were tested as arrival height and there was no obvious difference in results) above

the surface and the total run times was 120 hours for each backward trajectory and in time interval of 3 hours during the whole measurement period. The vertical motion was calculated using the default model selection, which used the meteorological model's vertical velocity fields. Angle distance (Sirois and Bottenheim, 1995) was selected to calculate clusters in this study.

To identify the impact of different air masses in a multiple linear regression model, WRF-FLEXPART (Stohl et al., 2005; Brioude et al., 2013) was used to obtain the clusters of particle trajectories reaching the Nam Co Station. 1000 particles were released per hour in the bottom 100 m surface layer above Nam Co Station and were tracked in backward mode for 4 days (de Foy et al., 2016a). Residence Time Analysis (RTA) (Ashbaugh et al., 1985) was used to create gridded fields representing the dominant transport paths of air masses impacting the measurement site (Wang et al., 2016; Wang et al., 2017). A k-means algorithm was used to classify the transport patterns into clusters (Wang et al., 2016). Six clusters were found to represent the dominant flow patterns to the Nam Co Station simulated using WRF-FLEXPART.

A tracer for stratospheric ozone incursions at the measurement site was obtained using the CAMx (Comprehensive Air-quality Model with eXtensions) v6.30 model (Ramboll Environ, 2016). The model initial and boundary conditions were obtained from ERA-Interim ozone fields, retaining only concentrations above 80 ppb and higher than 400 hPa. CAMx simulations were performed using the WRF medium and fine domains (domains 2 and 3) in nested mode for the full 4 year time series. In order to serve as a tracer for direct transport, there was no chemistry in the model and ozone was treated as a passive tracer. The resulting time series of the tracer concentration at the measurement site was used as input in the multi-linear regression model. This is similar to the procedure described in de Foy et al. (2014) to estimate the impact of the free troposphere on surface reactive mercury concentrations.

The ECMWF ERA-Interim data (Dee et al., 2011) was used to analyze the upper troposphere and lower stratosphere structures of the meridional cross-section over Nam Co Station.

2.4 Multiple Linear Regression Model

A Multiple Linear Regression (MLR) model was used in this study to quantify the main factors affecting hourly surface ozone concentrations. The method follows the description provided in de Foy et al. (2016b and 2016c). The inputs to the MLR model include meteorological parameters (wind speed, temperature, solar radiation and humidity), inter-annual variation factors, seasonal factors, diurnal factors, WRF boundary layer heights, WRF-FLEXPART trajectory clusters and the CAMx stratospheric ozone tracer. To obtain a normal distribution, the MLR model was applied to the logarithm of the ozone concentration offset by 10 ppb. For the WRF-FLEXPART clusters, a separate time series was constructed for each cluster, with

1 for the hours experiencing that particular cluster and 0 otherwise. The model estimated a coefficient corresponding to enhanced or decreased ozone concentrations for each cluster. The inputs to the model were normalized linearly except for the ozone tracer which was transformed log-normally with 0 offset. Because the results of Least-Squares methods are sensitive to outliers, an Iteratively Reweighted Least Squares (IRLS) procedure was used to screen them out. Measurement times when the model residual was greater than two standard deviations of all the residuals were excluded from the analysis. This was repeated iteratively until the method converged on a stable set of outliers (de Foy et al., 2016a).

Tests were performed with different variables and averaging times for each, including hourly data, running averages of 3, 8 and 24 hours, and smoothed variables using Kolmogorov-Zurbenko filters (Rao et al., 1997). For the boundary layer height as well as for the wind speed and direction, the variables were decomposed into quintiles with separate regression factors for each quintile in order to enable non-linear influences of these variables in the model. The variables to be included in the regression were obtained iteratively. At each iteration, the variable leading to the greatest increase in the square of Pearson's correlation coefficient was added to the inputs as long as the increase was greater than 0.005. Block-bootstrapping was used with a 24 hour block length to estimate the uncertainty in the results. 100 realizations of the final model were performed to obtained the standard deviation of the model uncertainties (de Foy et al., 2015).

2.5 Potential Source Contribution Function

The Potential Source Contribution Function (PSCF) assumes that back-trajectories arriving at times of higher mixing ratios likely point to the more significant pollution directions (Ashbaugh et al., 1985). PSCF has been applied in previous studies to locate air masses associated with high levels of surface ozone for different sites (Kaiser et al., 2007; Dimitriou and Kassomenos, 2015). In this study, PSCF was calculated by using trajectories which were calculated by HYSPLIT. The top of the model was set to 10000 m. The PSCF values for the grid cells in the study domain are based on a count of the trajectory segment (hourly trajectory positions) that terminate within each cell (Ashbaugh et al., 1985). Let n_{ij} be the total number of endpoints that fall in the *ij*th cell during whole simulation period. Let m_{ij} represents the number of points in the same cell that have arrival times at the sampling site corresponding to surface ozone mixing ratios higher than a set criterion. In this study, we calculate the PSCF based on trajectories corresponding to concentrations that exceed the mean level of surface ozone. The PSCF value for the *ij*th cell is then defined as:

$$\mathrm{PSCF}_{ij} = \frac{\mathrm{m}_{ij}}{\mathrm{n}_{ij}}$$

The PSCF value can be interpreted as the conditional probability that the ozone mixing ratios at measurement site is

greater than the mean mixing ratios if the air parcel passes though the *ij*th cell before arriving at the measurement site. Cells with high PSCF values are associated with the arrival of air parcels at the receptor site that have pollutant mixing ratios that exceed the criterion value. These cells are indicative of areas of 'high potential' contributions for the chemical constituent.

Identical $PSCF_{ij}$ values can be obtained from cells with very different counts of back-trajectory points (e.g. grid cell A with m*ij*=5000 and n*ij*=10000 and grid cell B with m*ij* = 5 and n*ij* = 10). In this extreme situation grid cell A has 1000 times more air parcels passing through than grid cell B. Because of the sparse particle count in grid cell B, the PSCF values are more uncertain. To account for the uncertainty due to low values of n*ij*, the PSCF values were scaled by a weighting function W_{ij} (Polissar et al., 1999). The weighting function reduced the PSCF values when the total number of the endpoints in a cell was less than about three times the average value of the end points per each cell. In this case, W_{ij} was set as follows:

$$Wij \begin{cases} 1.00 & n_{ij} > 3N_{ave} \\ 0.70 & 3N_{ave} > n_{ij} > 1.5N_{ave} \\ 0.42 & 1.5N_{ave} > n_{ij} > N_{ave} \\ 0.05 & N_{ave} > n_{ij} \end{cases}$$

where N_{ave} represents the mean n_{ij} of all grid cells. The weighted PSCF values were obtained by multiplying the original PSCF values by the weighting factor.

3 Surface ozone behavior at Nam Co Station

3.1 Mean mixing ratio

The mean surface ozone mixing ratio at Nam Co Station during the entire observational period was 47.6 ± 11.6 ppb, and the yearly average surface ozone mixing ratio was between 46.0 and 48.9 ppb (Table 1). During the whole monitoring period, the lowest hourly mixing ratio at Nam Co Station was 10.1 ppb, which was observed on December 3rd, 2011; and the highest hourly mixing ratio was 94.7 ppb, which was recorded on June 11th, 2011, resulting in a range of ~85 ppb.

The mean surface ozone mixing ratio at Nam Co Station was within the reference range reported for the Himalayas and Tibetan Plateau, and it was higher than the ratios for the two nearest urban sites: Lhasa (Ran et al., 2014) and Dangxiong (Lin et al., 2015); and comparable to of two sites on the edge of the Tibetan Plateau: Waliguan Station (Xu et al., 2011) and NCO-P (5079 m) (Cristofanelli et al., 2010) (see Fig. 1 for station locations). Surface ozone mixing ratios at Nam Co as well as other sites over the Tibetan Plateau were generally higher than the range of 20-45 ppb measured at background sites in the mid-latitudes of the Northern Hemispheres. This was in agreement with the higher concentrations typically seen at sites located in the free troposphere (Vingarzan, 2004).

3.2 Seasonal pattern

Every month considered in this study had more than 400 hours of available data (valid data for each month >56%). The overall trends of surface ozone at Nam Co Station showed similar annual cycles with slight variations (Fig. S1). The monthly average mixing ratios of ozone from 2011 to 2015 at Nam Co Station showed clear seasonal features (Fig. 2): 1) remarkably high values in the late spring-early summer; 2) low values in the winter; 3) little fluctuation during the remainder of the year except for the late spring-early summer and 4) a small peak around October in the second half of the year. Three winter months (December, January and February) had the lowest monthly mean surface ozone mixing ratios (41.0±7.6 ppb – 41.5±7.0 ppb) of the year, with variations smaller than 0.5 ppb. Monthly mean surface ozone mixing ratios increased from February to March by ~3.5 ppb, and a sharp increase from 44.5±10.4 ppb to 54.7±11.6 ppb occurred in March-April. The monthly mean mixing ratios remained above 54 ppb for the next 3 months (April, May and June), with the highest monthly mean mixing ratios occurring in May (58.6±12.2 ppb). After a large decrease in June-July (from 55.5±12.7 ppb to 44.9±11.9 ppb), the monthly mean mixing ratios of surface ozone during the second half of the year remained at low levels (ranging from 41.5±7.0 ppb to 48.0±8.6 ppb), with a small increase in October.

3.3 Diurnal variation

The diurnal cycles at Nam Co Station showed low ozone mixing ratios at night and high ozone mixing ratios during the day, with a unimodal pattern. After a rapid increase during the morning (8:00-11:00) of 6 ppb, the surface ozone mixing ratio at Nam Co continued to increase until reaching a maximum at 18:00 (53.2±10.9 ppb); it then decreased continuously to its lowest level at 8:00 the next day. Field observations revealed that the ozone mixing ratios reached an average of 50.6±10.9 ppb during the day (9:00-20:00) and an average of 44.6±11.2 ppb during the night and early morning (21:00-8:00).

All seasons displayed similar diurnal ozone mixing ratio cycles at Nam Co Station (Fig. 3). The diurnal cycle shift from low level at night to high level during the daytime was generally characterized by early shifts in the spring and the summer and late shifts in the winter, which was most likely related to seasonal differences in sunrise times. Relatively large diurnal amplitudes were observed in the spring, with much smaller diurnal amplitudes observed during the summer, the autumn and the winter.

4 Factors affecting surface ozone variation at Nam Co Station

4.1 Impact of factors on seasonal variation

An iterative procedure was used to include the variables that contributed the most to the correlation coefficient of the multi-linear regression model for hourly surface ozone. This model included scaling factors for each year in the time series as well as sine and cosine terms with periods of 12 and 6 months to account for seasonality. Individual factors were further included for each hour of the day except for 12:00 and 13:00 BJT which were taken as the baseline. Factors for the local wind speed and direction were included by quintile for wind speeds and quartile for wind directions leading to 20 factors. For the boundary layer height quintiles were used. The best fit was obtained by using the 3-hour running average of wind variables and the minimum 3-hour boundary layer height. 6 factors were included for each of the particle trajectory clusters. Temperature and specific humidity (q, g/kg) were both found to improve the model. Because these vary on both the diurnal and seasonal time scale, the Kolmogorov-Zurbenko filter was used to separate each into 2 time series. The seasonal component used 5 passes of a 13-point moving average (Rao et al., 1997). The diurnal component was the difference between the hourly and the seasonal time series. For the ozone tracer, the best fit was obtained by using the Kolmogorov-Zurbenko seasonal average of the hourly CAMx tracer.

Table 2 showed that this model had 27,310 hourly data points of which 26,005 were retained by the IRLS procedure. The correlation coefficient (r) was 0.77 for the entire time series and 0.81 without the outliers. The time series of the model was shown in Fig. 4 and the scatter plot between the measurements and the model were shown in Fig. S2. Note that because stratospheric incursions are seasonal, with a maximum in the spring, there was covariance between the stratospheric tracer and the seasonal signal. Uncertainties in the estimate of the contribution from one of these therefore impact the estimate from the other.

A log-transformed model provided estimates of the contribution to the variance in the hourly ozone by different factors. Because some of these co-vary, we grouped them together in order to calculate the fraction of variation as shown in Table 2. The stratospheric ozone tracer from the CAMx model contributed 18.2±2.6% of the ozone variance at the site and the WRF-FLEXPART wind transport clusters (Fig. S3) contributed 6.5±1.7%. Local winds accounted for 31.0±1.8%, seasonal variations (including the 12 and 6-month sine and cosine terms, and the seasonal temperature and humidity terms) accounted for 35.3±3.0%, diurnal signals (including the hourly terms and the diurnal temperature and humidity signals) accounted for 7.4±0.8%, the annual signal for 1.5±0.5% and the WRF boundary layer height for 0.1±0.1% of the variance. Fig. S4 showed the histograms of the contribution terms as well as the covariance of the results by group, as determined by the block-bootstrapped method.

Figure 4 showed the contribution of the stratospheric ozone tracer and the seasonal signal. Because the model was log-transformed, these were expressed as percentage enhancements or reductions relative to the model determined baseline. The model suggested that up to 20% of the ozone variability was due to stratospheric incursions, and that these can lead to enhancements of surface of ozone of 150% of the hourly standard deviation.

As a separate test, the regression model was performed with linear transformations instead of log-transformations. The results were shown in Table 2. Although the fit was not as good, the results were remarkably similar. The contribution of the stratospheric tracer was lower, mainly because there were individual peaks which had a larger influence in the linearly transformed model than in the log-transformed model. Fig. S5 (corresponding to Fig. 4) showed the linear results. Although the mean contribution of the stratospheric tracer to surface ozone concentrations was only 1 ppb over the entire time series, it can reach above 20 ppb during specific events in the spring.

Potential vorticity from the ERA-Interim model at 500 hPa, which was near the surface at Nam Co, was not found to contribute to the simulated ozone time series. However, at 350 hPa a positive correlation was found. The correlation was even larger if we took the potential vorticity at 350 hPa above the Himalayas. Total column ozone correlated more weakly with surface ozone than potential vorticity and was not found to improve the regression model. As for potential vorticity, the correlation coefficient for total column ozone was higher above the Himalayas than at the measurement site. Fig. S6 showed the 24-hour running average of the surface ozone and the stratospheric tracer at the measurement site, and the total column ozone and the potential vorticity from ERA-Interim above the Himalayas.

We performed a separate model run where we replaced the stratospheric tracer with the potential vorticity time series at 350 hPa above the Himalayas. The model found the best fit using the Kolmogorov-Zurbenko seasonally filtered time series of potential vorticity. The model had a slightly lower correlation coefficient, and lower contribution of the potential vorticity tracer (5.8%) than the model using the CAMx stratospheric tracer. This suggests that the CAMx stratospheric tracer was a better indicator of stratospheric ozone incursions than the time series of potential vorticity.

The regression model was also performed by season, as shown in Table S1. This shows that the largest stratospheric incursions occurred in the spring (Mar, Apr, May) with 20% contribution to ozone variation, and did not impact surface ozone in the fall (Sep, Oct, Nov). The air mass transport clusters accounted for nearly 10% of the ozone variation in the summer (Jun, Jul, Aug) but very little otherwise.

In order to visualize the transport of ozone from the stratosphere to the troposphere, we analyzed the upper troposphere

and lower stratosphere structures of the meridional cross-section of monthly mean ERA-Interim data above Nam Co Station (Fig. 5). In the spring (Mar, Apr and May), the dynamical tropopause (identified by the isolines of 1 and 2 potential vorticity unit) exhibited a folded structure over the Tibetan Plateau. This tropopause folding can lead to a downward transport of ozone from the stratosphere to the troposphere. Tropopause folding happened in the southern Tibetan Plateau and close to Nam Co Station in the spring. Cosmogenic ^{35}S results (Lin et al., 2016) also indicated that in the spring, Nam Co was affected by aged stratospheric air originating over the Himalayas rather than being affected by transport from fresh stratospheric air masses directly above Nam Co Station. The larger diurnal amplitude of surface ozone in the spring than other seasons (Fig. 3, mentioned in section 3.3) may be related to four factors: (1) position of STE hot spot; (2) frequency of STE; (3) PBLH at Nam Co Station and (4) solar radiation at Nam Co Station. In the spring, plots of tropopause folding suggest that STE mostly happens in the southern Tibetan Plateau which is close to Nam Co Station and that STE even happens right above Nam Co Station. Furthermore, PBLH at Nam Co Station was higher in the spring than during the rest of the year. The higher PBLH in the spring facilitated the impact of downward transport from the stratosphere to Nam Co Station. The spring also has more intense solar radiation than the summer because the Monsoon leads to increased cloudiness in the summer. The Pearson's correlation coefficient between monthly SWD and surface ozone was ~0.93 in 2012 (2012 was selected because it had a more complete dataset than the other years) (Fig. 6) indicating that monthly surface ozone variability at Nam Co Station was associated with solar radiation. This was expected as increased solar radiation promotes the photochemical production of surface ozone in the spring, which is similar to the mechanism at other background sites (Monks 2000). Consequently, more photochemical production of ozone is expected in the spring. In the summer (Jun, Jul and Aug), the jet core moved to the northern Tibetan Plateau and tropopause folding was relatively farther from Nam Co Station than those in the spring. Consequently, there was a smaller impact of stratospheric air at Nam Co Station. With tropopause folding further north in the summer, the air masses from the northern Tibetan Plateau may contribute more to the surface ozone levels at Nam Co Station than the air masses from the southern Tibetan Plateau. In the autumn (Sep, Oct and Nov) and the winter (Der, Jan and Feb), the heights of folding were higher than those in the spring and the summer; and the PBLHs in the autumn and the winter were much lower than those in the spring and the summer. Furthermore, SWD in the autumn and the winter were weaker than those in the spring and the summer. These factors contributed to the relatively low level of surface ozone at Nam Co Station in the autumn and the winter.

4.2 Impacts of photochemical production and vertical mixing on diurnal variation

In the regression model, solar radiation was not selected as an input by the automatic procedure based on the improvement

in the correlation coefficient of the model due to individual time series. The solar radiation time series does match the surface ozone concentration, but it was not as good as a match as local winds and the diurnal profile. This is probably due to the time delay between the maximum ozone concentration and the maximum solar radiation. Hourly average SWD showed a positive correlation with hourly average surface ozone (correlation coefficient=0.77) which indicated that the potential of local ozone formation by photochemical production during the daytime contributed to the peak in the afternoon (Wang et al., 2006). Wind speed and PBLH are also generally regarded as the main factors influencing the diurnal cycle of surface ozone. High wind speed was found to covary with turbulent downward mixing in previous studies in the Tibetan Plateau (Tang et al., 2002; Ma et al., 2014; Lin et al., 2015). There was a lake-land breeze influencing Nam Co Station and the wind speed in the daytime was higher than those at night (Fig. S7). Hourly average wind speed and PBLH at Nam Co Station showed positive correlation with hourly average surface ozone (Fig. 7). The correlation coefficient between hourly average surface ozone and hourly average wind speed was 0.95 and the correlation coefficient between hourly average surface ozone and hourly average PBLH was 0.92. These results indicated that high level of surface ozone was associated with high wind speed and high PBLH.

5 Synthesis comparison of surface ozone variation across the Tibetan Plateau and beyond

5.1 Diurnal variation

Diurnal surface ozone patterns varied among sites across the Tibetan Plateau (Fig. 8). Nam Co Station, Xianggelila, Lhasa and Dangxiong showed similar diurnal surface ozone patterns as discussed in section 4.2.

Diurnal surface ozone at NCO-P showed different patterns in different seasons (Fig. 8), and thermal circulation was the main influential factor (Cristofanelli et al., 2010). Surface ozone mixing ratio at Waliguan experienced a minimum around noon and a maximum at night (Fig. 8), which is indicative of a mountain-valley breeze (local anabatic and catabatic winds) (Xue et al., 2011). Specifically, more boundary layer air affected Waliguan and resulted in lower surface ozone at noon; whereas at night, more air masses from free tropospheric increased the surface ozone level (Xu et al., 2011). It should be noted that the amplitudes in the diurnal variations at Waliguan were much smaller than those at other sites.

In all, diurnal surface ozone variations across the Tibetan Plateau were generally controlled by site-specific meteorological conditions and photochemical production. Sites located in plains or valleys exhibited daytime maxima of ozone associated with vertical mixing and photochemical production whereas mountain top sites experienced daytime ozone minima associated with up-slope flow of low-ozone air.

5.2 Seasonal variation

The seasonal variation of surface ozone mixing ratios at different sites around the world is influenced by many factors

including: stratospheric intrusion, photochemical production, long-range transport of ozone or its precursors, local vertical mixing and even deposition (Vingarzan, 2004; Ordónez et al., 2005; Tang et al., 2009; Reidmiller et al., 2009; Cristofanelli et al., 2010; Langner et al., 2012; Ma et al., 2014; Lin et al., 2015; Ran et al., 2014; Xu et al., 2011; Macdonald et al., 2011; Pochanart et al., 2003; Derwent et al., 2016; Lin et al., 2014; Tarasova et al., 2009; Gilge et al., 2010; Wang et al., 2011; Wang et al., 2009; Zhu et al., 2004; Zhang et al, 2015; Nagashima et al., 2010). The seasonal variation of ozone at sites across the Tibetan Plateau and at the ridge of Himalayas can be divided into the Summer-maximum and Spring-maximum type based on the location of the sites:

A) The northern Tibetan Plateau: Summer-maximum type.

In the northern Tibetan Plateau (Waliguan site), surface ozone showed a maximum in the summer and a minimum in the winter (Fig. 9A). The summer maximum of surface ozone at Waliguan was linked to the impact of a high ozone band between 35°N-45°N over 70°E-125°E (Zhu et al., 2004). Similarly, Qinghai Lake site also showed a maximum in the summer (Shen et al., 2014). Horizontal and vertical transports have been regarded as major contributor to surface ozone at these two sites (Zhu et al., 2004; Shen et al., 2014).

B) The central Tibetan Plateau: Spring-maximum type.

Sites in the central Tibetan Plateau including Nam Co Station showed maximum ozone during the late spring-early summer and relatively low levels in the remainder of year (Fig. 9B), corresponding to the Spring-maximum type. Compared with the surface ozone levels at Nam Co Station, those at Lhasa and Dangxiong were much lower. It is possible that the local NOx emissions in these two urban regions reduce the average ozone on the urban scale. A study at Dangxiong revealed that the greater rainfall in the summer caused the surface ozone levels to remain relatively low during the warm period (July-September) (Lin et al., 2015). At Lhasa, photochemistry was the main factor affecting surface ozone in the spring and the summer, whereas transport largely contributed to the observed ozone mixing ratios in the autumn and the winter (Ran et al., 2014). Large-scale background of surface ozone in the spring considered an important influence on Dangxiong and Lhasa in the spring (Lin et al., 2015; Ran et al., 2014).

C) The southern Tibetan Plateau and the southern ridge of the Himalayas: Spring-maximum type.

In the southern Tibetan Plateau and the southern ridge of the Himalayas, Xianggelila and NCO-P each had a single surface ozone peak in the spring (pre-monsoon) and a minimum in the summer (monsoon) with a difference between the two exceeding 30 ppb. This pattern is different from those of the northern and central Tibetan Plateau (Fig. 9C). At NCO-P, frequent

stratospheric intrusions were recorded in all seasons except during the monsoon season (Cristofanelli et al., 2010). A similar frequency of downward transport was identified at Xianggelila, including less frequent intrusions in the summer (Ma et al., 2014).

5.3 Backward trajectories and PSCF results of surface ozone at Nam Co Station

Backward trajectories and PSCF were utilized to identify the air masses associated with high levels of surface ozone at Nam Co Station and to assess the regional representativity of surface ozone at Nam Co. In the spring, the air masses that arrived at Nam Co Station were predominantly from the west and from the south, and the 3-D clusters indicated that the air masses traveled through the Himalayas before reaching Nam Co Station (Fig. 10). Cristofanelli et al. (2010), Putero et al. (2016) and Chen et al. (2011) found that the frequency of stratospheric intrusions in the Himalayas was high in the spring, and slightly lower than during the winter. This was confirmed by analysis of the ERA-Interim data set showed that the seasonal average ozone flux from the stratosphere to the troposphere in the Himalayas was high in the spring (Škerlak et al., 2014). The contribution of polluted air masses in driving ozone variability at the southern ridge of the Himalayas was remarkable in the spring and it may also have an effect on the level of surface ozone at Nam Co Station through transport. In the summer, there are more backward trajectories coming from the northern Tibetan Plateau than in the other seasons (Fig. 10). During the summer, the northern Tibetan Plateau is the hot spot of stratosphere-to-troposphere ozone flux; and during autumn this flux remains higher than the one in the southern Tibetan Plateau (Škerlak et al., 2014). The summer peak of surface ozone at Waliguan also suggests that the northern Tibetan Plateau and northwestern China (a band between 35°N-45°N over 70°E-125°E) have their highest level of surface ozone in the summer (Zhu et al., 2004).

HYSPLIT backward trajectories arriving at Nam Co Station in the spring and the summer were classified in 6 clusters respectively (Fig. 11). In the spring, clusters which came from the southern Tibetan Plateau had higher mean surface ozone levels than clusters which came from the northern Tibetan Plateau. Air masses transported from the Himalayas therefore led to higher concentrations of surface ozone at Nam Co Station. The higher level of surface ozone at NCO-P (Cristofanelli et al., 2010) than at Nam Co Station in the spring may also be the result of this. In the summer, clusters from the northern Tibetan Plateau had higher mean surface ozone levels than clusters which came from the southern Tibetan Plateau. The air masses that arrived at Nam Co Station from the northern Tibetan Plateau and northwestern China by horizontal wind transport likely resulted in the higher ozone concentrations at Nam Co Station in the summer.

Using PSCF, we have identified air masses associated with higher surface ozone at Nam Co Station in different seasons (Fig. 12) and throughout the measurement periods (Fig. S8). The Himalayas region to the south of Nam Co Station and South

Asian countries including Nepal, India Pakistan, Bangladesh and Bhutan had high PSCF weight values in both spring and summer. The large areas of northwestern China, including the northern Tibetan Plateau, were the regions in additional potential high PSCF weight values in the summer. The PSCF values at both the southern Tibetan Plateau and the northern Tibetan Plateau in the autumn were smaller than those in the spring and the summer. In the autumn, the inland Tibetan Plateau seems to have a larger impact on the study site than regions more on the edge of the Tibetan Plateau. In the winter, no obvious region was identified, which was likely due to low surface ozone mixing ratios in all these areas. Considering the results in section 4.3, PSCF probably picked up the contribution from STE as a signal from the south in the spring and from the north in the summer.

5.4 Implication for measurement and study of surface ozone in the inland Tibetan Plateau and beyond

The changes of the atmospheric environment of the Tibetan Plateau are of universal concern due to its rapid responses and feedbacks to regional and global climate changes. The Tibetan Plateau covers vast areas with varied topography; however, comprehensive monitoring sites are few and sporadically distributed. Analysis of atmospheric composition at Waliguan in the north and Everest in the south of the Tibetan Plateau have shown that they are representative of high-altitude background sites for the entire Tibetan Plateau. It is noteworthy that the Tibetan Plateau, as a whole, is primarily regulated by the interplay of the Indian summer monsoon and the westerlies; and the atmospheric environment over the Tibetan Plateau is heterogeneous. Mount Everest is representative of the Himalayas on the southern edge of the Tibetan Plateau and is the sentinel of South Asia where anthropogenic atmospheric pollution has been increasingly recognized as disturbing the high mountain regions (Decesari et al., 2010; Maione et al., 2011; Putero et al., 2014). In addition, Mount Everest has been identified as a hotspot for stratospheric- tropospheric exchange (Cristofanelli et al., 2010; Škerlak et al., 2014) where the surface ozone is elevated from the baseline during the spring due to frequent stratospheric intrusions. Waliguan, in the northern Tibetan Plateau, is occasionally influenced by regional polluted air masses (Zhu et al., 2004; Xue et al., 2011; Zhang et al., 2011). Its mountainous landform facilitates mountain-valley breezes and may sometimes pump up anthropogenic emissions especially during the winter (Xue et al., 2011). Nam Co Station, in the inland Tibetan Plateau, is distant from both South Asia and northwestern China, it has been found to be influenced by episodic long-range transport of air pollution from South Asia (Xia et al, 2011; Lüthi et al., 2015), evidenced by the study of aerosol and precipitation chemistry at Nam Co Station (Cong et al., 2007; Cong et al., 2010). As for surface ozone, Nam Co Station is less influenced by stratospheric intrusions directly than NCO-P, and is minimally influenced by local anthropogenic emission. It showed distinct seasonal and diurnal variation patterns as compared with those sites in the Himalayas and the northern Tibetan Plateau as presented earlier. Our measurements of surface ozone at Nam Co are essential baseline data of the inland Tibetan Plateau. More long-term measurements are needed to enable a better spatial

coverage and a comprehensive understanding of regional surface ozone variations and underlying influence mechanisms.

6 Summary

Surface ozone mixing ratios and meteorological parameters were continuously measured from January 2011 to October 2015 at Nam Co Station in the inland Tibetan Plateau. The inter-annual mixing ratios of surface ozone were stable with an average of 47.6±11.6 ppb throughout the monitoring period. The surface ozone mixing ratios at Nam Co Station were high in the spring and low in the winter. The diurnal cycle indicated that the ozone mixing ratio continued to increase after sunrise until sunset and was higher in the daytime than at night.

The baseline of surface ozone is mainly controlled by various natural factors. Downward transport of air masses, air masses from the southern Tibetan Plateau in the spring and from the northern Tibetan Plateau in the summer contributed to the elevated monthly concentrations of ozone at the surface. Diurnal peaks of surface ozone in the afternoon were associated with high SWD, high PBLH and high wind speed. The analysis suggests that stratospheric intrusions account for around 20% of the variability in surface ozone concentrations at Nam Co Station. Further analysis of tropopause folding suggest that Nam Co Station is affected by "aged" air masses associated with stratospheric intrusions transported from the southern and northern Tibetan Plateau, mainly during the spring and the summer, respectively.

Synthesis comparison of ozone variability at regional and hemispheric scales revealed that the seasonality of surface ozone at Nam Co Station is most similar to other background sites in the Northern Hemisphere, albeit with slightly higher fluctuations in the summer season due to infrequent occurrences of air mass transport from Northwest China. Surface ozone at Nam Co showed distinct seasonal and diurnal variation patterns as compared with those sites in the Himalayas and the northern Tibetan Plateau. The monthly maximum of surface ozone at Nam Co Station was later in the year than the sites in the southern Tibetan Plateau and the southern ridge of the Himalayas, but earlier than the sites in the northern Tibetan Plateau.

Our measurements provide a baseline of tropospheric ozone at a remote site in the Tibetan Plateau, and contribute to the understanding of ozone cycles and related physico-chemical and transport processes over the Tibetan Plateau. More long-term measurements of surface ozone at field sites covering the spatially extensive Tibetan Plateau are needed to improve our understanding of surface ozone variations and the underlying influence mechanisms.

Acknowledgements

The authors are grateful to NOAA for providing HYSPLIT model and GFS meteorological files. The authors thank Yaqiang Wang who is the developer of MeteoInfo and give selfless help. Finally, the authors would like to thank the editor and

referees of this manuscript for their helpful comments and suggestions. This study was supported by the National Natural Science Foundation of China (41371088, and 41630754) and the Strategic Priority Research Program (B) of the Chinese Academy of Sciences (XDB03030504).

References

Ashbaugh, L. L., Malm, W. C., and Sadeh, W. Z.: A residence time probability analysis of sulfur concentrations at Grand Canyon National Park, Atmospheric Environment (1967), 19, 1263-1270, 1985.

Brasseur, G., Orlando, J. J., and Tyndall, G. S.: Atmospheric chemistry and global change, Oxford University Press, 1999.

Brioude, J., Arnold, D., Stohl, A., Cassiani, M., Morton, D., Seibert, P., Angevine, W., Evan, S., Dingwell, A., and Fast, J. D.: The Lagrangian particle dispersion model FLEXPART-WRF version 3.1, Geoscientific Model Development, 6, 1889-1904, 2013.

Chameides, W., and Walker, J. C.: A photochemical theory of tropospheric ozone, Journal of Geophysical Research, 78, 8751-8760, 1973.

Chen, X., Ma, Y., Kelder, H., Su, Z., and Yang, K.: On the behaviour of the tropopause folding events over the Tibetan Plateau, Atmospheric Chemistry and Physics, 11, 5113-5122, 2011.

Cong, Z., Kang, S., Liu, X., and Wang, G.: Elemental composition of aerosol in the Nam Co region, Tibetan Plateau, during summer monsoon season, Atmospheric Environment, 41, 1180-1187, 2007.

Cong, Z., Kang, S., Smirnov, A., and Holben, B.: Aerosol optical properties at Nam Co, a remote site in central Tibetan Plateau, Atmospheric Research, 92, 42-48, 2009.

Cong, Z., Kang, S., Zhang, Y., and Li, X.: Atmospheric wet deposition of trace elements to central Tibetan Plateau, Applied Geochemistry, 25, 1415-1421, 2010.

Cooper, O. R., Parrish, D., Ziemke, J., Balashov, N., Cupeiro, M., Galbally, I., Gilge, S., Horowitz, L., Jensen, N., and Lamarque, J.-F.: Global distribution and trends of tropospheric ozone: An observation-based review, Elementa: Science of the Anthropocene, 2, 000029, 2014.

Cristofanelli, P., Bracci, A., Sprenger, M., Marinoni, A., Bonafè, U., Calzolari, F., Duchi, R., Laj, P., Pichon, J., and Roccato, F.: Tropospheric ozone variations at the Nepal Climate Observatory-Pyramid (Himalayas, 5079 m asl) and influence of deep stratospheric intrusion events, Atmospheric Chemistry and Physics, 10, 6537-6549, 2010.

Crutzen, P. J.: Photochemical reactions initiated by and influencing ozone in unpolluted tropospheric air, Tellus, 26, 47-57, 1974.

de Foy, B., Heo, J., and Schauer, J. J.: Estimation of direct emissions and atmospheric processing of reactive mercury using inverse modeling, Atmospheric environment, 85, 73-82, 2014.

de Foy, B., Cui, Y., Schauer, J., Janssen, M., Turner, J., and Wiedinmyer, C.: Estimating sources of elemental and organic carbon and their temporal emission patterns using a least squares inverse model and hourly measurements from the St.

Louis–Midwest supersite, Atmospheric Chemistry and Physics, 15, 2405-2427, 2015.

de Foy, B., Tong, Y., Yin, X., Zhang, W., Kang, S., Zhang, Q., Zhang, G., Wang, X., and Schauer, J. J.: First field-based atmospheric observation of the reduction of reactive mercury driven by sunlight, Atmospheric Environment, 134, 27-39, 2016a.

de Foy, B., Lu, Z., and Streets, D. G.: Impacts of control strategies, the Great Recession and weekday variations on NO 2 columns above North American cities, Atmospheric Environment, 138, 74-86, 2016b.

de Foy, B., Lu, Z., and Streets, D. G.: Satellite NO2 retrievals suggest China has exceeded its NOx reduction goals from the twelfth Five-Year Plan, Scientific Reports, 6, 2016c.

Decesari, S., Facchini, M., Carbone, C., Giulianelli, L., Rinaldi, M., Finessi, E., Fuzzi, S., Marinoni, A., Cristofanelli, P., and Duchi, R.: Chemical composition of PM 10 and PM 1 at the high-altitude Himalayan station Nepal Climate Observatory-Pyramid (NCO-P) (5079 m asl), Atmospheric Chemistry and Physics, 10, 4583-4596, 2010.

Dee, D., Uppala, S., Simmons, A., Berrisford, P., Poli, P., Kobayashi, S., Andrae, U., Balmaseda, M., Balsamo, G., and Bauer, P.: The ERA‐Interim reanalysis: Configuration and performance of the data assimilation system, Quarterly Journal of the royal meteorological society, 137, 553-597, 2011.

Derwent, R. G., Parrish, D. D., Galbally, I. E., Stevenson, D. S., Doherty, R. M., Young, P. J., and Shallcross, D. E.: Interhemispheric differences in seasonal cycles of tropospheric ozone in the marine boundary layer: Observation‐model comparisons, Journal of Geophysical Research: Atmospheres, 121, 2016.

Desqueyroux, H., Pujet, J.-C., Prosper, M., Squinazi, F., and Momas, I.: Short-term effects of low-level air pollution on respiratory health of adults suffering from moderate to severe asthma, Environmental research, 89, 29-37, 2002.

Dimitriou, K., and Kassomenos, P.: Three year study of tropospheric ozone with back trajectories at a metropolitan and a medium scale urban area in Greece, Science of The Total Environment, 502, 493-501, 2015.

Draxler, R. G., Parrish, D. D., Galbally, I. E., Stevenson, D. S., Doherty, R. M., Young, P. J., and Shallcross, D. E.: Interhemispheric differences in seasonal cycles of tropospheric ozone in the marine boundary layer: Observation‐model comparisons, Journal of Geophysical Research: Atmospheres, 121, 2016.

Draxler, R. R., and Rolph, G.: HYSPLIT (HYbrid Single-Particle Lagrangian Integrated Trajectory) model access via NOAA ARL READY website (http://www. arl. noaa. gov/ready/hysplit4. html). NOAA Air Resources Laboratory, Silver Spring, in, Md, 2003.

Fishman, J., and Crutzen, P. J.: The origin of ozone in the troposphere, 1978.

Gilge, S., Plass-Dülmer, C., Fricke, W., Kaiser, A., Ries, L., Buchmann, B., and Steinbacher, M.: Ozone, carbon monoxide and nitrogen oxides time series at four alpine GAW mountain stations in central Europe, Atmospheric Chemistry and Physics, 10, 12295-12316, 2010.

Huang, J., Kang, S., Zhang, Q., Yan, H., Guo, J., Jenkins, M. G., Zhang, G., and Wang, K.: Wet deposition of mercury at a remote site in the Tibetan Plateau: concentrations, speciation, and fluxes, Atmospheric environment, 62, 540-550, 2012.

Junge, C. E.: Global ozone budget and exchange between stratosphere and troposphere, Tellus, 14, 363-377, 1962.

Kaiser, A., Scheifinger, H., Spangl, W., Weiss, A., Gilge, S., Fricke, W., Ries, L., Cemas, D., and Jesenovec, B.: Transport of nitrogen oxides, carbon monoxide and ozone to the alpine global atmosphere watch stations Jungfraujoch (Switzerland),

Zugspitze and Hohenpeißenberg (Germany), Sonnblick (Austria) and Mt. Krvavec (Slovenia), Atmospheric Environment, 41, 9273-9287, 2007.

Kang, S., Yang, Y., Zhu, L., and Ma, Y.: Modern environmental processes and changes in the Nam Co basin, Tibetan Plateau, in, China: Beijing Meteorological Press, 2011.

Langner, J., Engardt, M., Baklanov, A., Christensen, J. H., Gauss, M., Geels, C., Hedegaard, G. B., Nuterman, R., Simpson, D., and Soares, J.: A multi-model study of impacts of climate change on surface ozone in Europe, Atmospheric Chemistry and Physics, 12, 10423-10440, 2012.

Li, C., Kang, S., Zhang, Q., and Kaspari, S.: Major ionic composition of precipitation in the Nam Co region, Central Tibetan Plateau, Atmospheric Research, 85, 351-360, 2007.

Lin, M., Horowitz, L. W., Oltmans, S. J., Fiore, A. M., and Fan, S.: Tropospheric ozone trends at Mauna Loa Observatory tied to decadal climate variability, Nature Geoscience, 7, 136-143, 2014.

Lin, M., Zhang, Z., Su, L., Hill‐Falkenthal, J., Priyadarshi, A., Zhang, Q., Zhang, G., Kang, S., Chan, C. Y., and Thiemens, M. H.: Resolving the impact of stratosphere‐to‐troposphere transport on the sulfur cycle and surface ozone over the Tibetan Plateau using a cosmogenic 35S tracer, Journal of Geophysical Research: Atmospheres, 121, 439-456, 2016.

Lin, W., Xu, X., Zheng, X., Dawa, J., Baima, C., and Ma, J.: Two-year measurements of surface ozone at Dangxiong, a remote highland site in the Tibetan Plateau, Journal of Environmental Sciences, 31, 133-145, 2015.

Liu, Y., Wang, Y., Pan, Y., and Piao, S.: Wet deposition of atmospheric inorganic nitrogen at five remote sites in the Tibetan Plateau, Atmospheric Chemistry and Physics, 15, 11683-11700, 2015.

Low, P., Davies, T., Kelly, P., and Farmer, G.: Trends in surface ozone at Hohenpeissenberg and Arkona, Journal of Geophysical Research: Atmospheres, 95, 22441-22453, 1990.

LRTAP, 2015. Mapping Critical Levels for Vegetation, Chapter III of Manual on methodologies and criteria for modelling and mapping critical loads and levels and air pollution effects, risks and trends. UNECE Convention on Long-range Transboundary Air Pollution

Lüthi, Z., Škerlak, B., Kim, S., Lauer, A., Mues, A., Rupakheti, M., and Kang, S.: Atmospheric brown clouds reach the Tibetan Plateau by crossing the Himalayas, Atmos. Chem. Phys, 15, 1-15, 2015.

Ma, J., Lin, W., Zheng, X., Xu, X., Li, Z., and Yang, L.: Influence of air mass downward transport on the variability of surface ozone at Xianggelila Regional Atmosphere Background Station, southwest China, Atmospheric Chemistry and Physics, 14, 5311-5325, 2014.

Ma, Y., Kang, S., Zhu, L., Xu, B., Tian, L., and Yao, T.: Roof of the world: Tibetan observation and research platform: Atmosphere-land Interaction over a heterogeneous landscape, Bulletin of the American Meteorological Society, 89, 1487-1492, 2008.

Macdonald, A., Anlauf, K., Leaitch, W., Chan, E., and Tarasick, D.: Interannual variability of ozone and carbon monoxide at the Whistler high elevation site: 2002–2006, Atmos. Chem. Phys, 11, 11431-11446, 2011.

Maione, M., Giostra, U., Arduini, J., Furlani, F., Bonasoni, P., Cristofanelli, P., Laj, P., and Vuillermoz, E.: Three-year observations of halocarbons at the Nepal Climate Observatory at Pyramid (NCO-P, 5079 m asl) on the Himalayan range, Atmospheric Chemistry and Physics, 11, 3431-3441, 2011.

Mauzerall, D. L., and Wang, X.: Protecting agricultural crops from the effects of tropospheric ozone exposure: reconciling science and standard setting in the United States, Europe, and Asia, Annual Review of Energy and the Environment, 26, 237-268, 2001.

Monks, P. S.: A review of the observations and origins of the spring ozone maximum, Atmospheric Environment, 34, 3545-3561, 2000.

Myhre, G., Shindell, D., Bréon, F.-M., Collins, W., Fuglestvedt, J., Huang, J., Koch, D., Lamarque, J.-F., Lee, D., and Mendoza, B.: Anthropogenic and natural radiative forcing, Climate change, 423, 2013.

Nagashima, T., Ohara, T., Sudo, K., and Akimoto, H.: The relative importance of various source regions on East Asian surface ozone, Atmospheric Chemistry and Physics, 10, 11305-11322, 2010.

Ordónez, C., Mathis, H., Furger, M., Henne, S., Hüglin, C., Staehelin, J., and Prévôt, A.: Changes of daily surface ozone maxima in Switzerland in all seasons from 1992 to 2002 and discussion of summer 2003, Atmospheric Chemistry and Physics, 5, 1187-1203, 2005.

Pochanart, P., Akimoto, H., Kajii, Y., Potemkin, V. M., and Khodzher, T. V.: Regional background ozone and carbon monoxide variations in remote Siberia/east Asia, Journal of Geophysical Research: Atmospheres, 108, 2003.

Polissar, A., Hopke, P., Paatero, P., Kaufmann, Y., Hall, D., Bodhaine, B., Dutton, E., and Harris, J.: The aerosol at Barrow, Alaska: long-term trends and source locations, Atmospheric Environment, 33, 2441-2458, 1999.

Putero, D., Landi, T., Cristofanelli, P., Marinoni, A., Laj, P., Duchi, R., Calzolari, F., Verza, G., and Bonasoni, P.: Influence of open vegetation fires on black carbon and ozone variability in the southern Himalayas (NCO-P, 5079 m asl), Environmental Pollution, 184, 597-604, 2014.

Putero, D., Cristofanelli, P., Sprenger, M., Škerlak, B., Tositti, L., and Bonasoni, P.: STEFLUX, a tool for investigating stratospheric intrusions: application to two WMO/GAW global stations, Atmospheric Chemistry and Physics, 16, 14203-14217, 2016.

Qiao, Q., and Zhang, Y.: Synoptic meteorology of the Tibetan Plateau and its effect on the near areas, in, China Meteorological Press, Beijing, 1994.

Ran, L., Lin, W., Deji, Y., La, B., Tsering, P., Xu, X., and Wang, W.: Surface gas pollutants in Lhasa, a highland city of Tibet–current levels and pollution implications, Atmospheric Chemistry and Physics, 14, 10721-10730, 2014.

Ramboll Environ, CAMx User's Guide: Comprehensive Air Quality Model with Extensions (CAMx) v6.30, March 2016.

Rao, S., Zurbenko, I., Neagu, R., Porter, P., Ku, J., and Henry, R.: Space and time scales in ambient ozone data, Bulletin of the American Meteorological Society, 78, 2153-2166, 1997.

Reidmiller, D., Fiore, A. M., Jaffe, D., Bergmann, D., Cuvelier, C., Dentener, F., Duncan, B. N., Folberth, G., Gauss, M., and Gong, S.: The influence of foreign vs. North American emissions on surface ozone in the US, Atmospheric Chemistry and Physics, 9, 5027-5042, 2009.

REVIHAAP: Review of evidence on health aspects of air pollution – REVIHAAP Project technical report. World Health Organization (WHO) Regional Office for Europe, Bonn. 2013.

Roelofs, G., Scheeren, H., Heland, J., Ziereis, H., and Lelieveld, J.: A model study of ozone in the eastern Mediterranean free troposphere during MINOS (August 2001), Atmospheric Chemistry and Physics, 3, 1199-1210, 2003.

Shen, Z., Cao, J., Zhang, L., Zhao, Z., Dong, J., Wang, L., Wang, Q., Li, G., Liu, S., and Zhang, Q.: Characteristics of surface O 3 over Qinghai Lake area in Northeast Tibetan Plateau, China, Science of the Total Environment, 500, 295-301, 2014.

Sirois, A., and Bottenheim, J. W.: Use of backward trajectories to interpret the 5 - year record of PAN and O3 ambient air concentrations at Kejimkujik National Park, Nova Scotia, Journal of Geophysical Research: Atmospheres, 100, 2867-2881, 1995.

Škerlak, B., Sprenger, M., and Wernli, H.: A global climatology of stratosphere–troposphere exchange using the ERA-Interim data set from 1979 to 2011, Atmos. Chem. Phys, 14, 913-937, 2014.

Stohl, A., Forster, C., Frank, A., Seibert, P., and Wotawa, G.: Technical note: The Lagrangian particle dispersion model FLEXPART version 6.2, Atmospheric Chemistry and Physics, 5, 2461-2474, 2005.

Tang, G., Li, X., Wang, Y., Xin, J., and Ren, X.: Surface ozone trend details and interpretations in Beijing, 2001–2006, Atmospheric Chemistry and Physics, 9, 8813-8823, 2009.

Tang, J., Zhou, L., Zheng, X., Zhou, X., Shi, G., and Suolang, D.: The observational study of surface ozone at Lhasa suburb in summer 1998, Act. Meteo. Sinica, 60, 221-229, 2002.

Tarasova, O., Senik, I., Sosonkin, M., Cui, J., Staehelin, J., and Prévôt, A.: Surface ozone at the Caucasian site Kislovodsk High Mountain Station and the Swiss Alpine site Jungfraujoch: data analysis and trends (1990–2006), Atmos. Chem. Phys, 9, 4157-4175, 2009.

U.S. EPA. Integrated Science Assessment (ISA) of Ozone and Related Photochemical Oxidants (Final Report, Feb 2013). U.S. Environmental Protection Agency, Washington, DC, EPA/600/R-10/076F, 2013.

Vecchi, R., and Valli, G.: Ozone assessment in the southern part of the Alps, Atmospheric Environment, 33, 97-109, 1998.

Vingarzan, R.: A review of surface ozone background levels and trends, Atmospheric Environment, 38, 3431-3442, 2004.

Wang, T., Wei, X., Ding, A., Poon, S. C., Lam, K., Li, Y., Chan, L., and Anson, M.: Increasing surface ozone concentrations in the background atmosphere of Southern China, 1994-2007, Atmospheric Chemistry and Physics, 2009.

Wang, T., Wong, H., Tang, J., Ding, A., Wu, W., and Zhang, X.: On the origin of surface ozone and reactive nitrogen observed at a remote mountain site in the northeastern Qinghai - Tibetan Plateau, western China, Journal of geophysical research: atmospheres, 111, 2006.

Wang, Y., de Foy, B., Schauer, J. J., Olson, M. R., Zhang, Y., Li, Z., and Zhang, Y.: Impacts of regional transport on black carbon in Huairou, Beijing, China, Environmental Pollution, 221, 75-84, 2017.

Wang, Y., Zhang, Y., Hao, J., and Luo, M.: Seasonal and spatial variability of surface ozone over China: contributions from background and domestic pollution, Atmospheric Chemistry and Physics, 11, 3511-3525, 2011.

Wang, Y., Zhang, Y., Schauer, J. J., de Foy, B., Guo, B., and Zhang, Y.: Relative impact of emissions controls and meteorology on air pollution mitigation associated with the Asia-Pacific Economic Cooperation (APEC) conference in Beijing, China, Science of The Total Environment, 571, 1467-1476, 2016.

Wang, Y.: MeteoInfo: GIS software for meteorological data visualization and analysis, Meteorological Applications, 21, 360-368, 2014.

Wild, O., and Prather, M. J.: Global tropospheric ozone modeling: Quantifying errors due to grid resolution, Journal of Geophysical Research: Atmospheres, 111, 2006.

Wu, S., Mickley, L. J., Jacob, D. J., Logan, J. A., Yantosca, R. M., and Rind, D.: Why are there large differences between models in global budgets of tropospheric ozone?, Journal of Geophysical Research: Atmospheres, 112, 2007.

Xia, X., Zong, X., Cong, Z., Chen, H., Kang, S., and Wang, P.: Baseline continental aerosol over the central Tibetan plateau and a case study of aerosol transport from South Asia, Atmospheric environment, 45, 7370-7378, 2011.

Xu, W., Lin, W., Xu, X., Tang, J., Huang, J., Wu, H., and Zhang, X.: Long-term trends of surface ozone and its influencing factors at the Mt Waliguan GAW station, China–Part 1: Overall trends and characteristics, Atmospheric Chemistry and Physics, 16, 6191-6205, 2016.

Xu, X., Tang, J., and Lin, W.: The trend and variability of surface ozone at the global GAW station Mt. WALIGUAN, China, Second Tropospheric Ozone Workshop Tropospheric Ozone Changes: Observations, state of understanding and model performances", WMO/GAW report, WMO, Geneva, 2011, 49-55.

Xue, L., Wang, T., Zhang, J., Zhang, X., Poon, C., Ding, A., Zhou, X., Wu, W., Tang, J., and Zhang, Q.: Source of surface ozone and reactive nitrogen speciation at Mount Waliguan in western China: new insights from the 2006 summer study, Journal of geophysical research: atmospheres, 116, 2011.

Yao, T., Thompson, L. G., Mosbrugger, V., Zhang, F., Ma, Y., Luo, T., Xu, B., Yang, X., Joswiak, D. R., and Wang, W.: Third pole environment (TPE), Environmental Development, 3, 52-64, 2012.

Zhang, F., Zhou, L., Novelli, P., Worthy, D., Zellweger, C., Klausen, J., Ernst, M., Steinbacher, M., Cai, Y., and Xu, L.: Evaluation of in situ measurements of atmospheric carbon monoxide at Mount Waliguan, China, Atmospheric Chemistry and Physics, 11, 5195-5206, 2011.

Zhang, L., Jin, L., Zhao, T., Yin, Y., Zhu, B., Shan, Y., Guo, X., Tan, C., Gao, J., and Wang, H.: Diurnal variation of surface ozone in mountainous areas: Case study of Mt. Huang, East China, Science of The Total Environment, 538, 583-590, 2015.

Zhu, B., Akimoto, H., Wang, Z., Sudo, K., Tang, J., and Uno, I.: Why does surface ozone peak in summertime at Waliguan?, Geophysical research letters, 31, 2004.

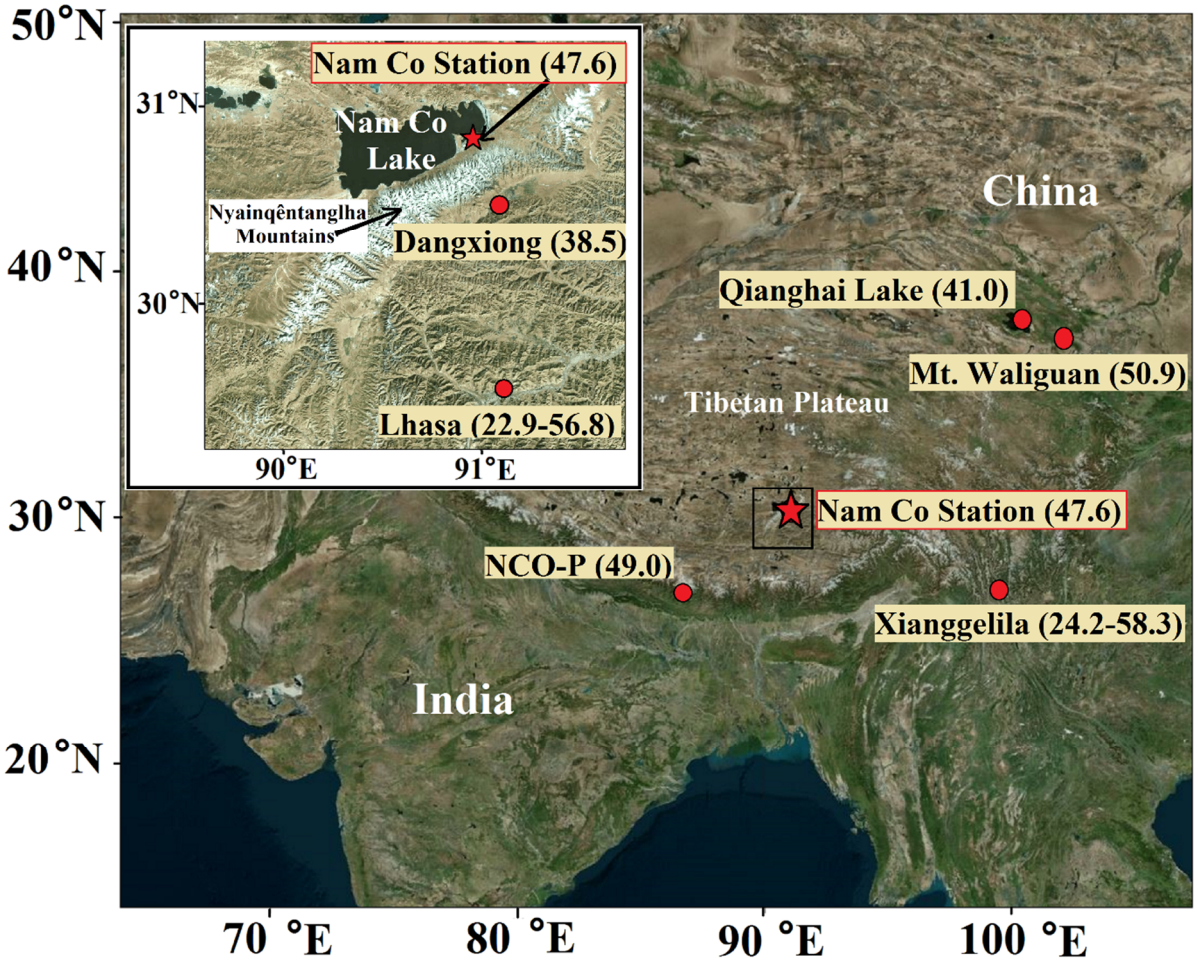

Fig. 1. Geographical location of Nam Co Station and other sites in the Tibetan Plateau. Values in the parenthesis refers to the average or range of surface ozone in ppb as obtained from Cristofanelli et al., 2010; Lin et al., 2015; Shen et al., 2014; Xu et al., 2011; Ma et al., 2014; Ran et al., 2014.

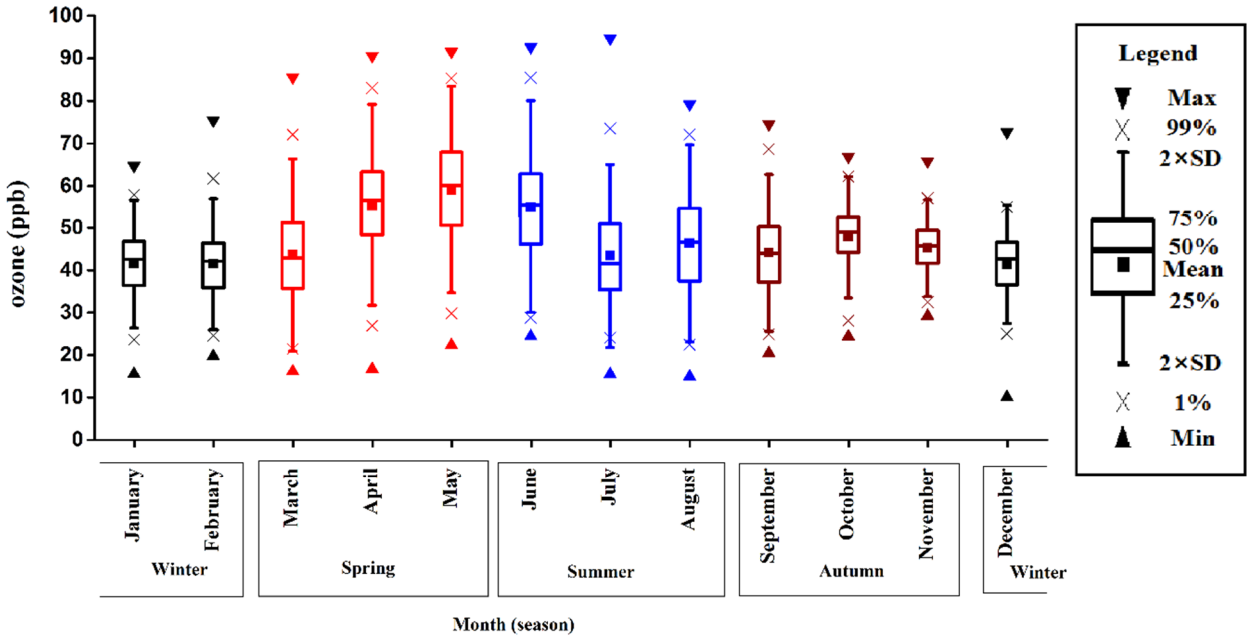

Fig. 2. Monthly average and statistical parameters of surface ozone at Nam Co Station during the whole measurement period (spring (MAM) in red; summer (JJA) in blue; autumn (SON) in dark red; winter (DJF) in black).

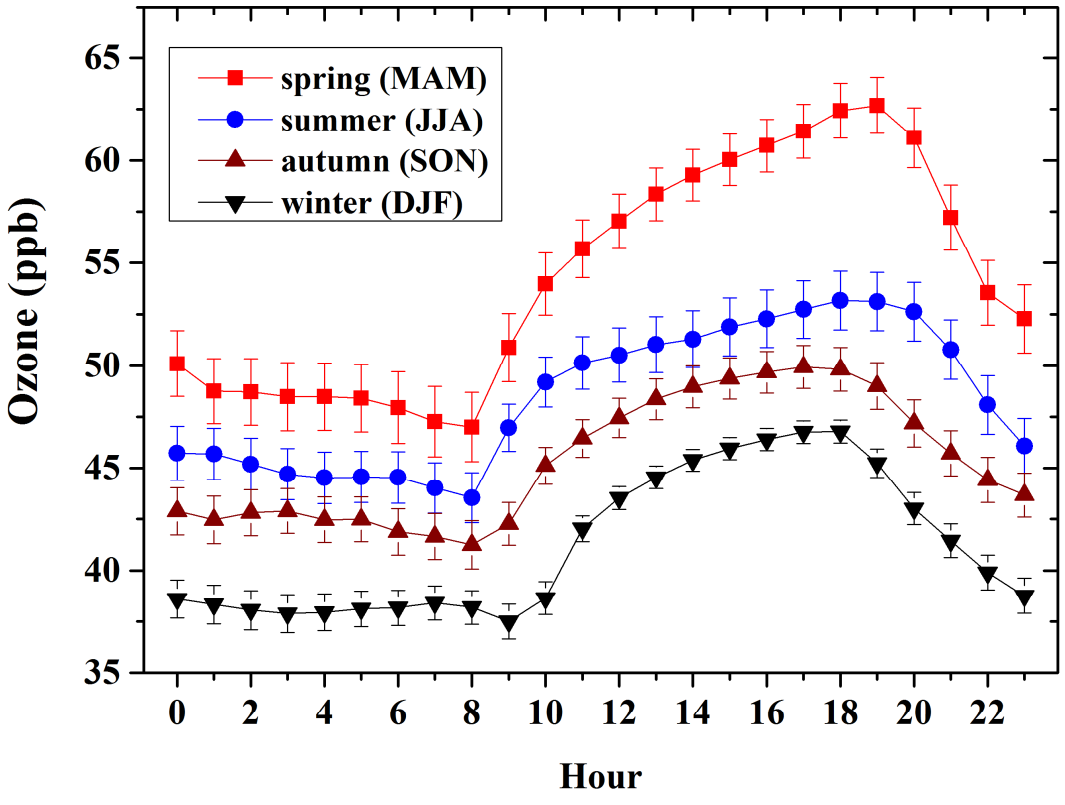

695 **Fig. 3. Diurnal profiles of average hourly surface ozone at Nam Co Station by seasons. Error bars are 95% confidence levels.**

700

705

710

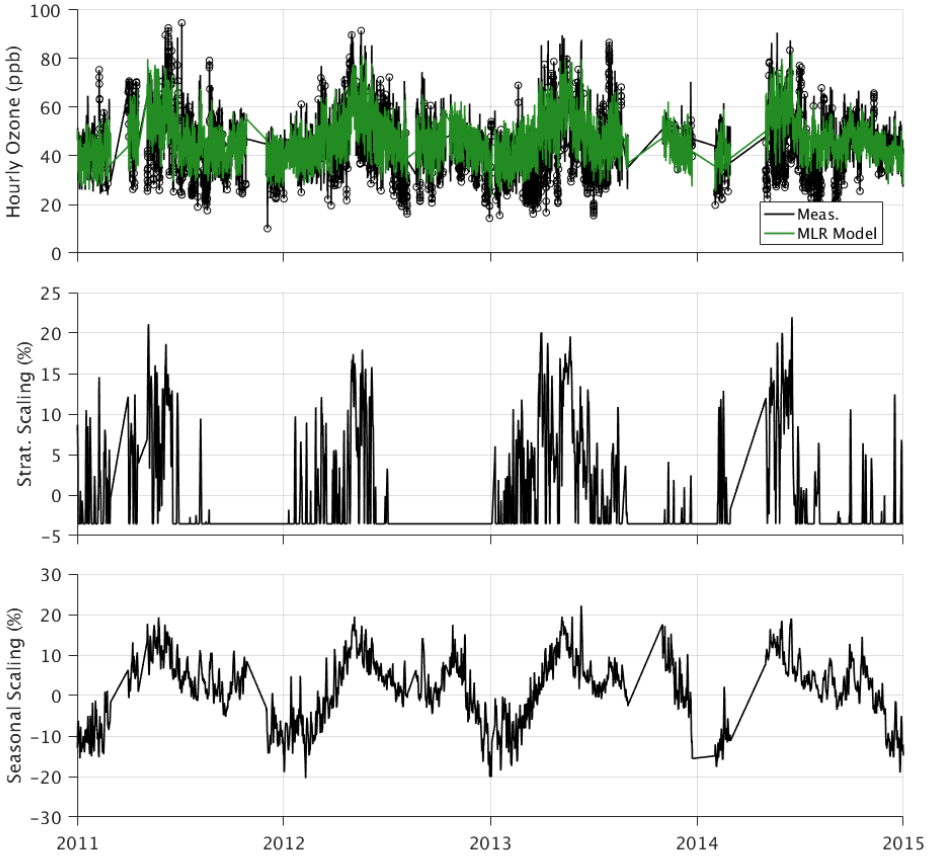

Fig. 4. Top: Surface hourly measurements of ozone at Nam Co (black) and multi-linear regression (MLR) model fit (green). Outliers rejected by the Iteratively Reweighted Least Squares Procedure are shown as circles. Middle: Scaling factor of the stratospheric ozone tracer simulated using CAMx. Bottom: Scaling factor due to the seasonal factors including the 12 and 6-month sine and cosines, and the seasonal temperature and specific humidity time series.

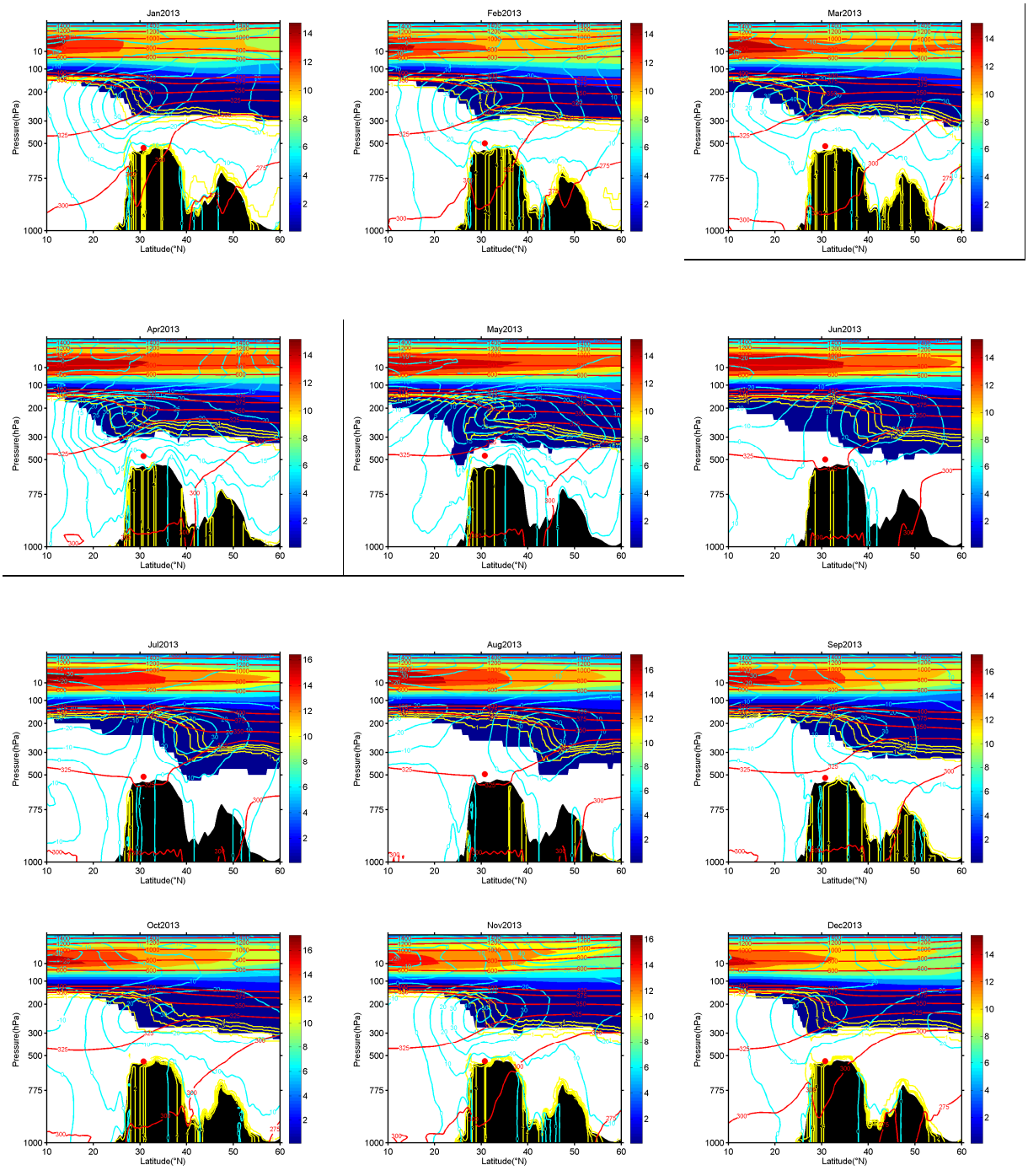

Fig. 5. Monthly mean meridional cross-section at 91° E (over Nam Co Station) at 20:00 UTC+8 in 2013, derived from ERA-Interim data, including zonal winds (cyan contours, m/s), potential vorticity (yellow lines, contours of 1, 2, 3, 4 potential vorticity unit), ozone (solid color, $\times 10^6$ kg/kg) and potential temperature (red contours, K). The color bar is the scale of ozone concentration. The area in black shows the cross section of the Tibetan Plateau terrain. The red dots show the position of the top of PBL.

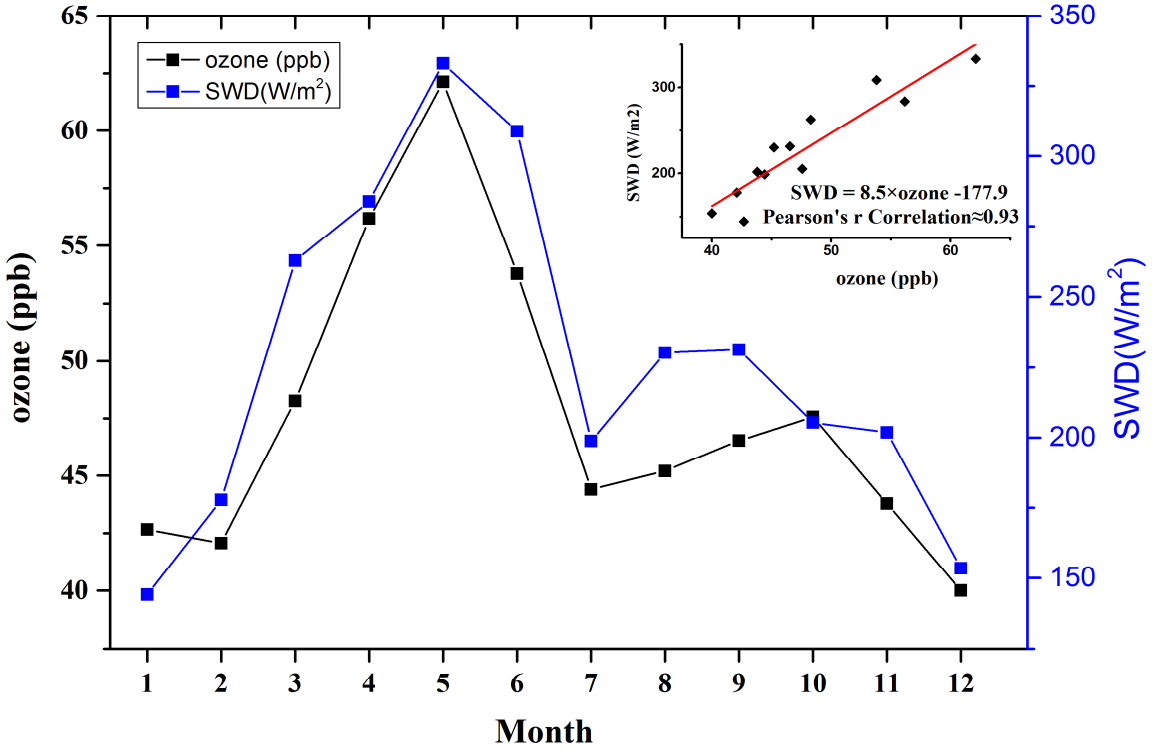

Fig. 6. Comparison between monthly average surface ozone (black) and monthly average SWD (downward shortwave radiation, blue) at Nam Co Station in 2012.

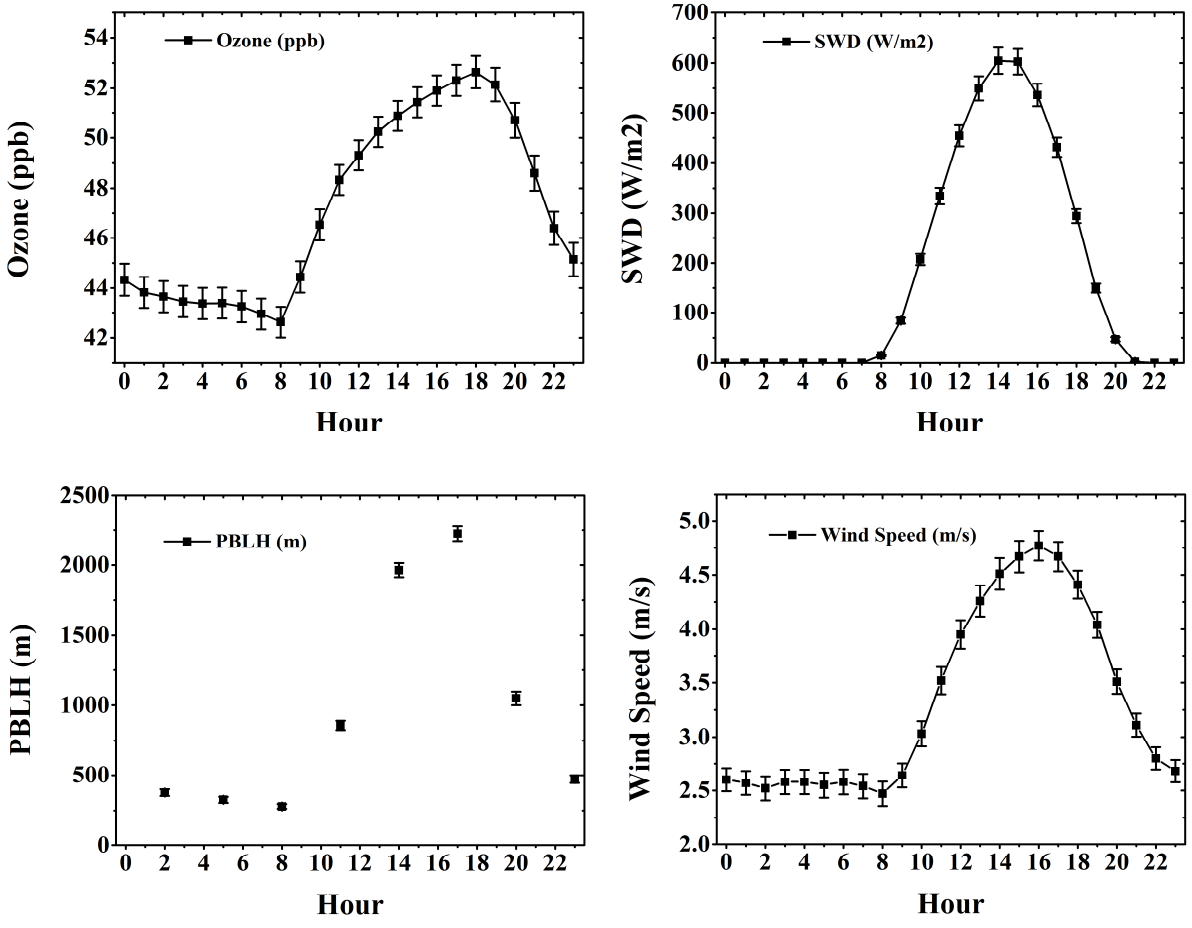

770

Fig. 7 Diurnal variations of hourly average of surface ozone, SWD (downward shortwave radiation), wind speed and PBLH (planetary boundary layer height) during the whole measurement period at Nam Co Station. Error bars are 95% confidence levels.

775

780

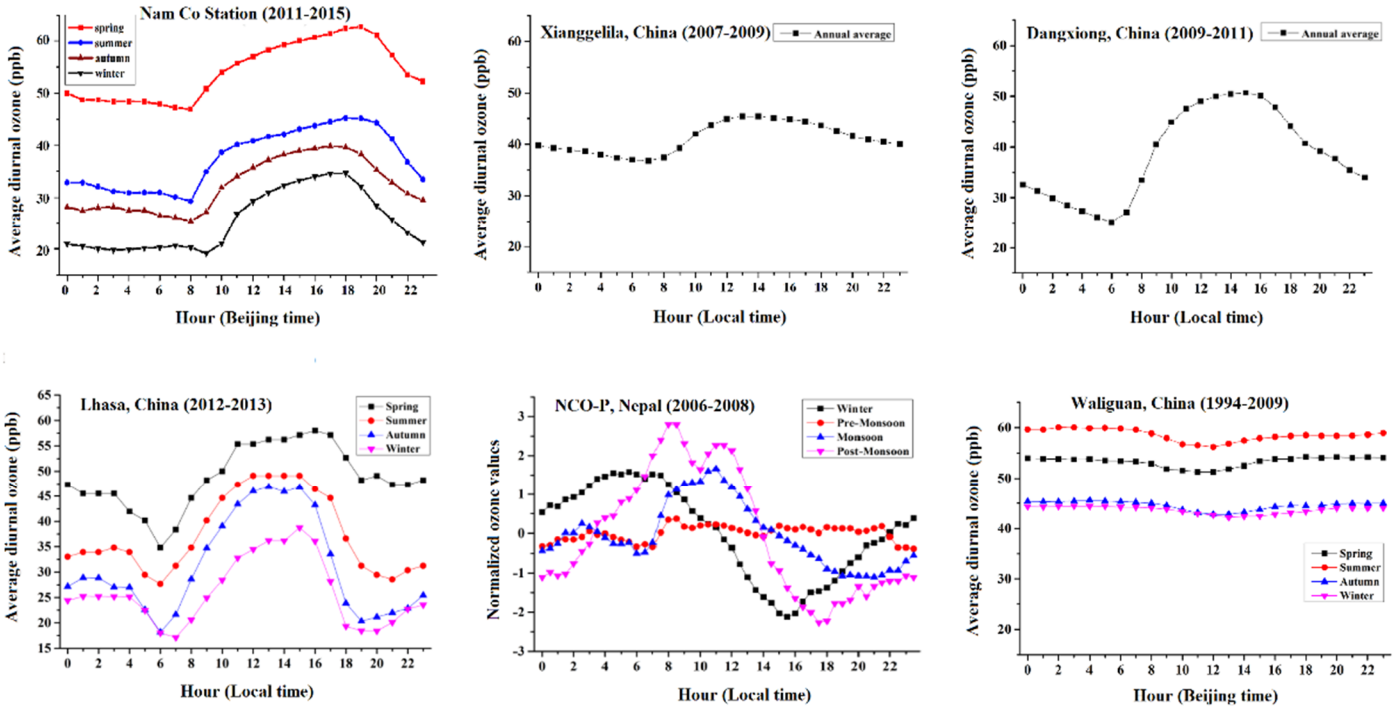

Fig. 8. Comparison of diurnal profiles of surface ozone concentration at different sites in the Tibetan Plateau (referred to Ma et al., 2014; Lin et al., 2015; Ran et al., 2014; Cristofanelli et al., 2010; Xu et al., 2011.) Measurement years at different sites are displayed in brackets.

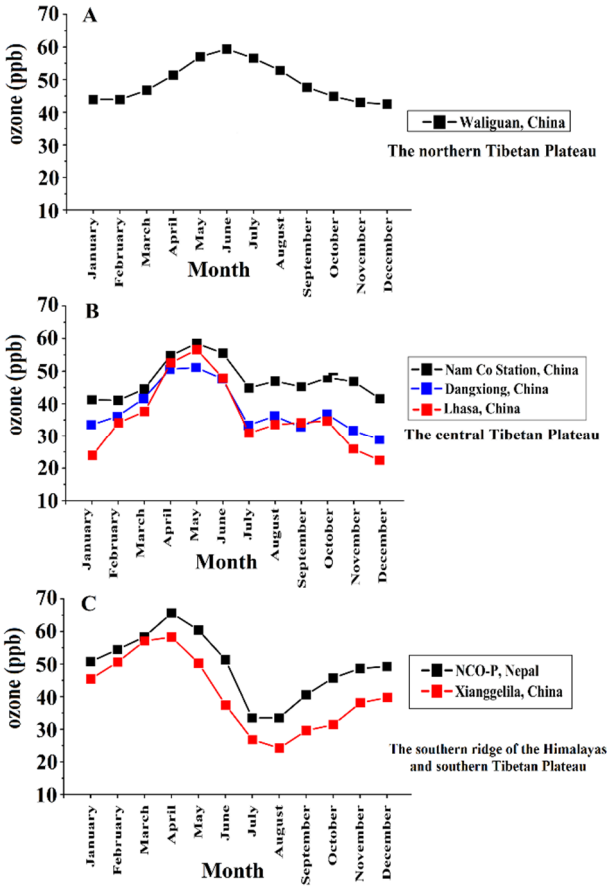

Fig. 9. Monthly variation of surface ozone at different sites in the Tibetan Plateau (right, A: The northern Tibetan Plateau: Summer-maximum type; B: The central Tibetan Plateau: Spring-maximum type and C: The southern Tibetan Plateau and the southern ridge of the Himalayas: Spring-maximum type) (referred to Ma et al., 2014; Lin et al., 2015; Ran et al., 2014; Cristofanelli et al., 2010; Zhu et al., 2004).

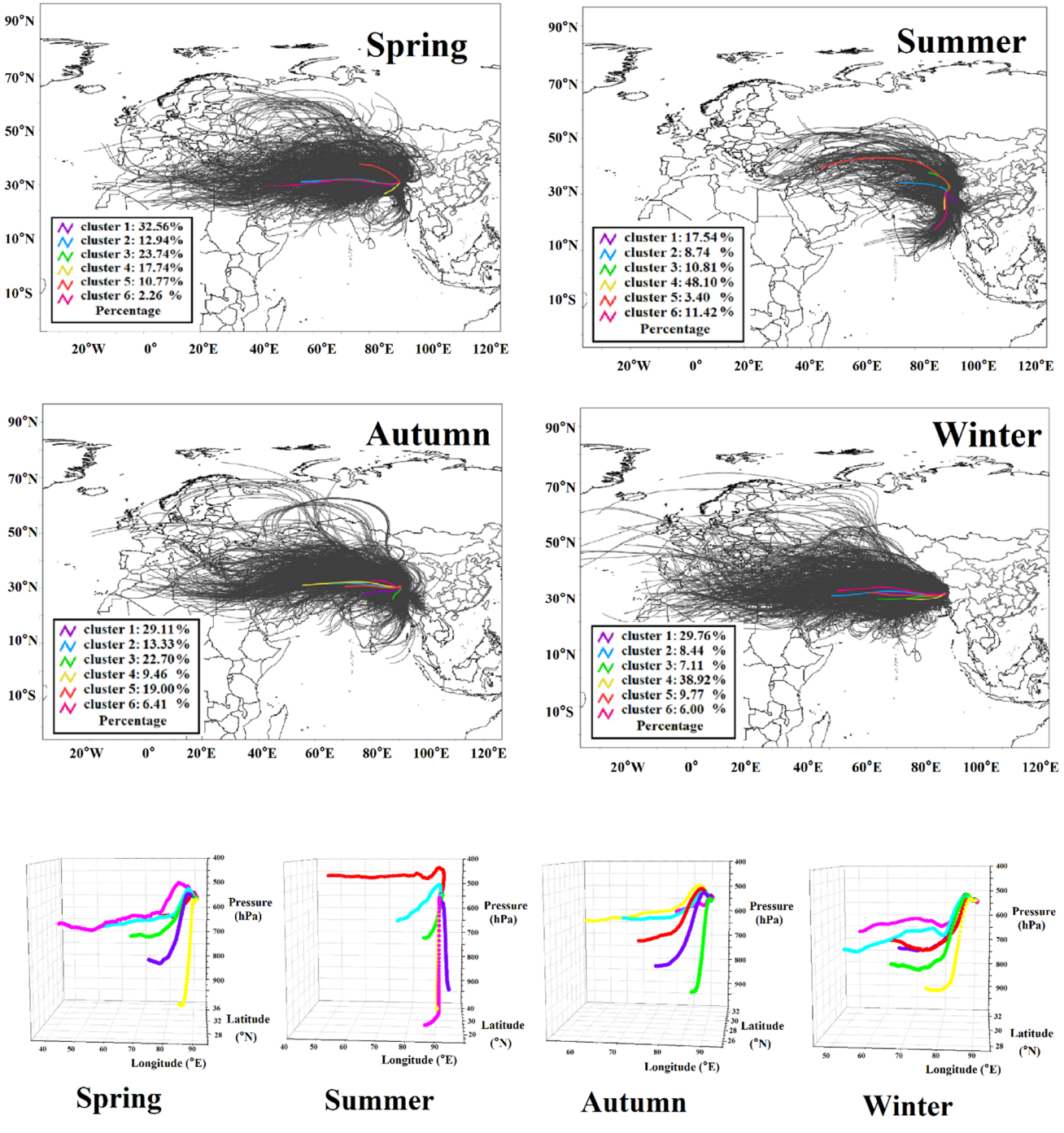

Fig. 10. Backward HYSPLIT trajectories for each measurement day (black lines in the maps), and mean back-trajectory for 6 HYSPLIT clusters (colored lines in the maps, 3D view shown on the right of the maps) arriving at Nam Co Station by season.

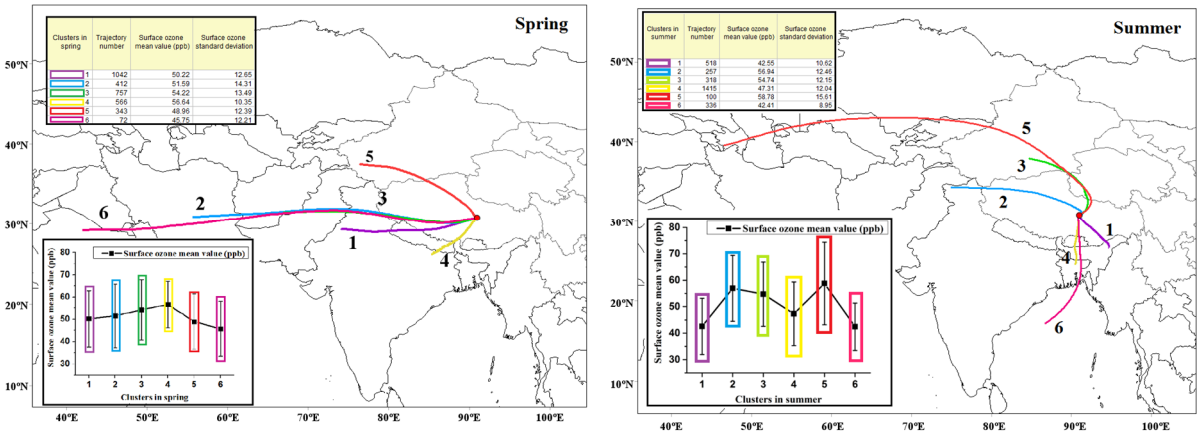

Fig. 11. Mean trajectory of 6 HYSPLIT clusters arriving at Nam Co Station in the spring and the summer. Subplot shows the range of surface ozone mixing ratios measured at Nam Co Station by cluster.

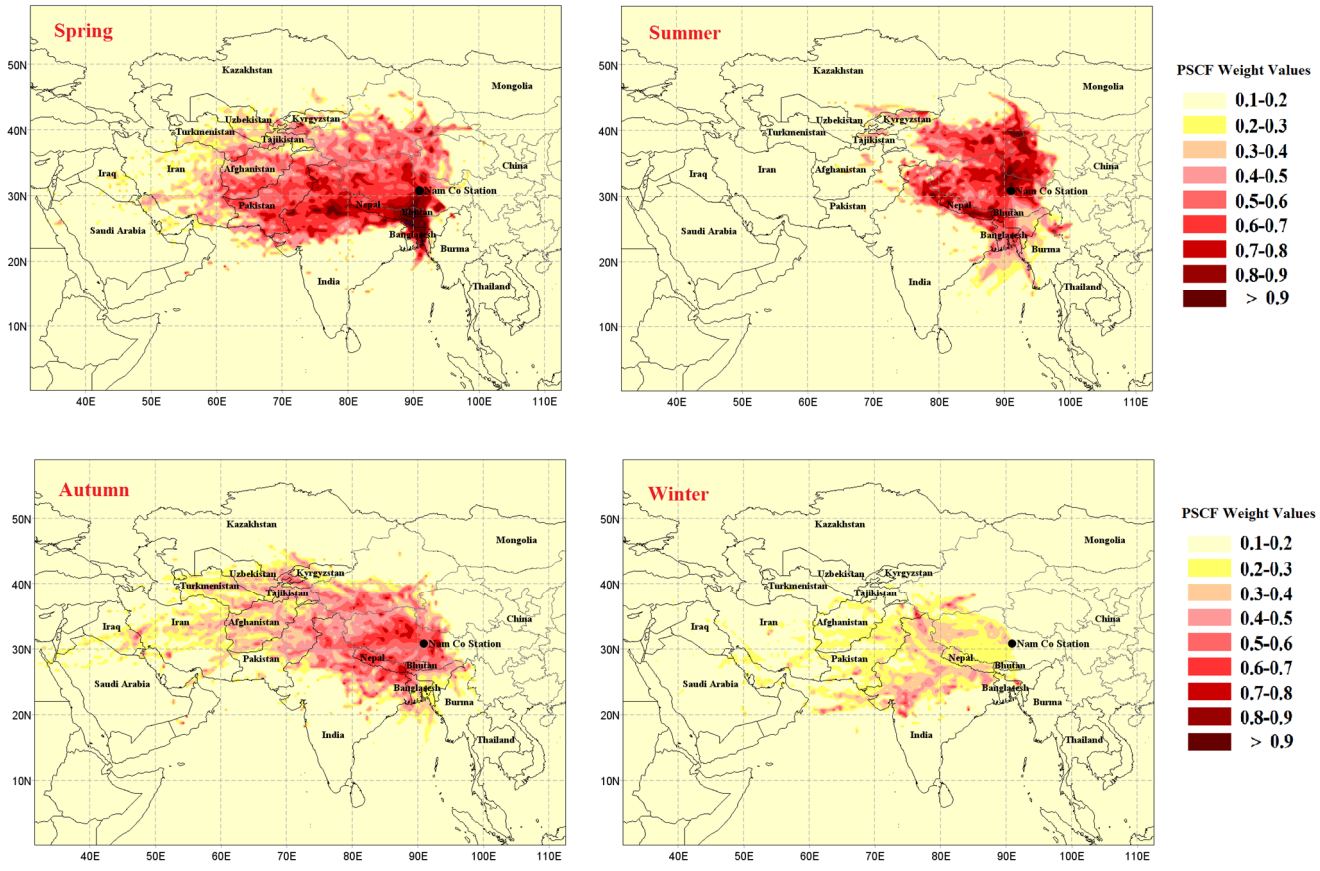

Fig. 12. Likely source areas of air mass associated with higher surface ozone concentrations at Nam Co Station by season identified using PSCF (Potential Source Contribution Function).

880 **Table 1. Statistical summary of surface ozone at Nam Co from 2011 to 2015.**

Year (valid time during whole year %)	Ozone (ppb)	Range (ppb)
2011 (75.25%)	46.0±12.1	10.1-94.7
2012 (90.30%)	48.1±11.4	14.3-91.5
2013 (75.90%)	47.5±12.3	15.5-89.7
2014 (70.05%)	47.5±10.6	14.9-90.8
2015 (66.21%)	48.9±12.0	17.3-94.7
Total	47.6±11.6	10.1-94.7

885

890

895

900

905

910

915

Table 2. Multi-Linear Regression Model for Hourly Ozone (2011-2014) for 3 different models.

Log, using CAMx Strat Tracer		**Linear, using CAMx Strat Tracer**		**Log, using ERA-Interim PV**	
No. All	27310	No. All	27310	No. All	27310
No. IRLS	26005	No. IRLS	25934	No. IRLS	25985
r (All)	0.77	r (All)	0.75	r (All)	0.75
r (IRLS)	0.81	r (IRLS)	0.79	r (IRLS)	0.80
		Contribution to Variance (%) by Group			
CAMx Tracers	18.2	CAMx Tracers	12.5	PV	5.8
WRF-FLEXPART Clusters	6.5	WRF-FLEXPART Clusters	6.8	WRF-FLEXPART Clusters	6.4
Local Winds	31.0	Local Winds	28.6	Local Winds	29.4
Seasonal Signal	35.3	Seasonal Signal	44.2	Seasonal Signal	52.1
Diurnal Signal	7.4	Diurnal Signal	6.7	Diurnal Signal	5.7
Annual Signal	1.5	Annual Signal	0.7	Annual Signal	0.5
WRF PBLH	0.1	WRF PBLH	0.4	WRF PBLH	0.2

920